Soybean protein isolate/chitosan complex-rutin microcapsules

Shuai Dong,[a] Shu-Min Hu,[a] Si-Jia Yu,[a] Shaobo Zhou,[b,a] and Tao Zhou *[a]

[a.] *School of Food Science and Biotechnology, Zhejiang Gongshang University, Xiasha, Hangzhou, Zhejiang, 310018, P. R. China*

[b.] *School of Science, Faculty of Engineering and Science, University of Greenwich, Central Avenue, Chatham ME4 4TB, UK*

*Corresponding authors.

Tel: (+86) 571 28008976. E-mail address: taozhou@zjgsu.edu.cn (T. Zhou).

Abstract: Rutin is a flavonoid polyphenol with excellent biological activity, but due to its instability and poor water solubility, the utilization rate is reduced *in vivo*. Preparation of rutin microcapsules from soybean protein isolate (SPI) and chitosan hydrochloride (CHC) by composite coacervation can improve this restriction. The optimal preparation conditions were as follows: the volume ratio of CHC/SPI 1:8, pH 6, and total concentration of CHC and SPI 2%. The rutin encapsulation rate and loading capacity of the microcapsules were 90.34% and 0.51% under optimal conditions. The SPI-CHC-rutin (SCR) microcapsules had a gel mesh structure and good thermal stability, and the system was stable and homogeneous after 12 d storage. During in vitro digestion, the release rates of SCR microcapsules in simulated gastric and intestinal fluids were 16.97% and 76.53%, respectively, achieving a targeted release of rutin in intestinal fluids; and the digested products were found to exhibit superior antioxidant activity to that of free rutin digests, indicating a good protection of microencapsulation on the bioactivity of rutin. Overall, SCR microcapsules developed in this study effectively enhanced the bioavailability of rutin. The present work provides a promising delivery system for natural compounds with low bioavailability and stability.

Keywords: rutin; soybean protein isolate; chitosan

1. Introduction

Rutin is a flavonoid, also known as rutoside or quercetin 3-rutinoside. It has significant pharmacological effects, such as antioxidant, anti-inflammatory, and hypolipidemic activities [1]. However, its bioavailability and stability are relatively low, due to its sensitive to temperature, pH, light and oxygen. It has poor water solubility and short biological half-life [2]. These greatly limit its application in the fields of food and medicine. Therefore, there is an increasingly interest to develop the methods to improve its stability and water solubility in order to achieve its bioactive effect.

The drug delivery system can improve the biological efficacy, water solubility and sensory properties of bioactive ingredients, protect them from gastric digestion, and release them in the intestine [3]. The delivery systems based on proteins and polysaccharides can be realized by complex coacervation, which refers to the self-aggregation between two or more biopolymers via electrostatic interaction [4]. However, selection of protein and polysaccharide is crucial in order to achieve ideal encapsulation efficiency and targeted release in intestinal tract. Soybean protein is the primary supply of plant-based protein and is widely consumed by diverse populations worldwide, due to its highest protein quality among plant proteins and positive health effects [5]. Soybean protein isolate (SPI) is amphoteric and can interact with small bioactive molecules through hydrophobic interactions, hydrogen bonding, and disulfide bonds [6], and has been used for loading β-carotenoid [7], vanillin, resveratrol [8], and other active substances. Encapsulation of small hydrophobic molecules by the complex coacervation with SPI and polysaccharide has also been reported [9]. Chitosan

hydrochloride (CHC) is a water-soluble product of chitosan by protonation modification with hydrochloric acid. Chitosan (CS) has been widely used in the delivery and controlled release of functional compounds. The delivery systems formed by different kinds of proteins and polysaccharides have great differences in structure and properties. The conditions for the construction of delivery systems, such as temperature, pH, and polysaccharide/protein ratio, have great effects on the properties of delivery systems [8]. There have been some reports on the complexation of SPI and CS, and the use of SPI/CS complexes in delivery systems. The SPI/CS complexes have been demonstrated to effectively stabilize emulsions [10,11], and improve the stability of bioactive molecules by microencapsulation [12]. Therefore, SPI/CS complexes could have potential application in delivery systems. However, there are few studies on release profiles of bioactive ingredients microcapsules based on the complex coacervation of SPI and CS. In addition, use of CHC for complexation with SPI is more convenient for practical manipulation due to its good water solubility compared with CS. In order to develop a delivery system for improving the bioavailability and targeted release of rutin, in this work, the formation conditions of SPI/CHC complex coacervates were optimized, and rutin-loaded microcapsules were prepared using SPI/CHC complex as wall material. The physical properties, storage stability and rutin release behavior in a simulated gastrointestinal tract of the rutin-loaded microcapsules were also investigated.

2. Materials and methods

2.1. Materials

The SPI was purchased from Zhengzhou Qihuadun Chemical Products Co., LTD., the CHC (degree of deacetylation 80-95%) was purchased from Shanghai Maclin Biochemical Technology Co., LTD. Pepsin (1:1500) from porcine gastric mucosa, and pancreatin (USP) from porcine pancreas were purchased from Shanghai Aladdin Reagent Co., LTD. All chemicals and solvents were of analytical grade.

2.2. Preparation of SPI-CHC composite

SPI solution (4%) was prepared by mixing with deionized water and continuously stirring for 30 min [13]. CHC solution (1%) was prepared by dissolving in deionized water and magnetic stirring at room temperature for 1 h. The above-mentioned solutions were stored at 4°C before use. The SPI and CHC solutions were mixed at a ratio of 1:1, 1:2, 1:4, 1:8 and 1:16 (v/v), and the mixed solution was homogenized using a vortex oscillator for 10 min, followed by ultrasonic treatment (30 min). The resulting solution was equilibrated in a refrigerator for 24 h, and then was adjusted to different pH (2-9). The turbidity, zeta-potential and particle size of these solutions were monitored.

Turbidity of the SPI-CHC (SC) composite solutions with different pH values was determined by measuring the absorbance values of the solutions at a wavelength of 600 nm using a UV-Vis spectrophotometer. Turbidity was calculated using equation (1), where I_t is the transmitted light intensity and I_0 is the incident light intensity.

$$\text{Turbidity} = -\ln\frac{I_t}{I_0} \qquad (1)$$

Zeta-potential measurement: The zeta- potential of the solutions was measured at 298K using the electrophoretic light scattering mode on a laser particle size analyzer (Zetasizer Nano-ZS, Marvern, UK).

Particle size measurement: The particle size distribution and poly-dispersity index (PDI) of particles in the SPI, CHC and SC composite solutions at different pH values were measured by the dynamic light scattering mode in an ALV/CGS-3 integrated laser scattering instrument (ALV, Germany).

2.3. Preparation of SPI-CHC-rutin (SCR) microcapsules

SCR microcapsules were prepared by complex coacervation method according to the literature with modifications [14]. An ethanolic solution of rutin was dispersed into SPI solution, and mixed evenly by ultrasonic treatment for 20 min. Ethanol was then removed by rotary evaporator, and the CHC solution was added. After stirring at 60℃ for 30 min, the solution was adjusted to pH 6. The solution was vibrated for 10 min using the vortex oscillator, then freeze-dried to yield SCR microcapsule powder.

2.4. Determination of the encapsulation efficacy of rutin

SCR microcapsule powder (0.5g) was added into 10 mL ethanol, and the suspension was centrifuged at 10000 rpm for 20 min, the supernatant was collected and analyzed for free rutin content using spectrophotometry at 362 nm. SCR microcapsule powder (0.5g) was suspended in 10 mL of ethanol and sonicated (60 ℃, 40kHz) for 30 min to extract encapsulated rutin from SCR microcapsule powder. After centrifugation for 10 min, and the yielding supernatant was analyzed for the total rutin content. The encapsulation efficiency (EE) and loading rate (LR) of rutin in the SCR microcapsules were calculated using equations (2) and (3), respectively [15]

$$EE\ (\%) = (\text{Total rutin} - \text{free rutin}) \times 100/\text{Total rutin} \quad (2)$$

$$LR\ \% = (\text{Total rutin} - \text{free rutin}) \times 100/\text{Total weight of SCR powder} \quad (3)$$

2.5. Characterization of SCR microcapsules

2.5.1 Fourier transform infrared spectroscopy (FT-IR) analysis

FT-IR spectra of SPI, CHC, SC, RUT and SCR nanoparticle powders were recorded with KBr pellets on a NICOLET-380 infrared spectrometer (Thermo Fisher, USA) in the wavenumber range of 400–4000 cm^{-1} [16].

2.5.2 Differential scanning colorimetry (DSC)

The thermal behaviors of samples (SPI, CHC, SC, rutin, SPI-rutin (SR) and SCR microcapsules) were analyzed using a DSC [17]. Samples (2–3 mg) were hermetically sealed in aluminum pans and were scanned at a rate of 10 ℃/min from 20 to 300 °C. Data were analyzed using the TA Instruments Universal Analysis 2000 software.

2.5.3 Scanning electron microscopy (SEM)

The microstructural characteristics of SPI, CHC, SC and SCR lyophilized powder were studied using a Zeiss Sigma 300 ultra-high resolution scanning electron microscope. Before scanning with the electron microscope, the samples were sprayed with gold and then fixed on a short aluminum rod with the help of double-sided adhesive for recording the micrographs of samples.

2.6. Storage stability of SCR microcapsules

Based on the result of particle size and PDI determination at different pH values, SC complex and SCR microcapsule lyophilized powders (0.1 g) were dispersed in 30 mL of PBS buffer (pH 3) at a concentration of 0.5% (w/v), sonicated for 25 min until no obvious flocculent was observed. The samples were stored in a refrigerator at 4 ºC for 12 days, and their turbidity changes were measured by UV spectrophotometer at 600

nm at 3 day-intervals. Particle size and zeta potential were measured by dynamic light scatterer.

2.7. *In vitro* simulated digestion of SCR microcapsules

Referring to a reported method [18], simulated gastric juice (prepared by dissolving 1 g pepsin in 100 mL NaCl (0.03 M), followed by adjusting pH to 2.0 with 1.0 mol/L HCl) and simulated intestinal juice (1 g trypsin was dissolved in PBS solution (0.2mol/L), followed by adjusting pH to 8.0 with 0.1M NaOH). Digestion models were used to assess *in vitro* release of rutin from SCR particles. In brief, SCR powder (200 mg) was added to the simulated gastric juice (20 mL), after adjusting its pH to 2.0, it was incubated in a shaking table (100 rpm) at 37 °C to simulate gastric digestion (0-2h). During digestion, 2 mL of digestive fluid was collected every 0.5 h, and the same amount of simulated gastric juice was supplemented. After 2 h incubation, 20 mL of simulated intestinal fluid was added, the yielding mixture was adjusted to pH 8.0, and incubated for 4 h under the same conditions. The digestion solution (2 mL) was collected at 0.5h-intervals and re-supplemented with an equal volume of simulated intestinal fluid. The supernatant of the collected samples obtained by centrifugation was used for measuring the release of rutin at 360 nm. The release of rutin in SR samples was evaluated under the same conditions as SCR powder.

2.8. Retention of antioxidant activity during *in vitro* simulated digestion

In order to examine the protective effect of microencapsulation on the biological activities of lutin during digestion, the antioxidant activity of free rutin, SCR and SR after digestion was investigated. In short, free rutin, the SCR and SR samples containing

same amount of rutin (0.2 mg/mL) were digested as described above. The antioxidant activities of free rutin, SCR and SR digestion solutions by simulated gastrointestinal fluids were studied by determining their DPPH (1, 1- diphenyl-2-picrylhydrazil) and ABTS ((2, 2-azino-bis (3-ethylbenzthiazoline-6-sulfonic acid)) scavenging abilities. The determination of DPPH and ABTS scavenging abilities were performed as described by Wang et al. [19].

2.9. Statistical analysis

All the experiments were conducted at least three parallels. The experimental results were statistically analyzed using variance test analysis (SPSS Statistics 19 software). Significances of the differences between the groups with different treatments were examined using t-test. The difference was considered to be significant if $p < 0.05$.

3. Results and discussion

3.1 Influence of CHC/SPI ratio and pH on the interaction between SPI and CHC

Fig.1a shows the turbidity changes of the CHC/SPI composite solutions with different CHC/SPI ratios at different pH values. It has been demonstrated that the mass ratio of polysaccharide to protein has a great influence on the formation of polysaccharide/protein complexes [20]. As shown in Fig. 1a, when the CHC/SPI ratio was changed from 1:1 to 1:8, the turbidity curve moved towards a lower pH value, the optimal turbidity value gradually increased and reached the maximum when the ratio was 1:8. In this case, the sugar chain of CHC was saturated and absorbed by SPI, and the formation of complex aggregates reached the maximum. When the CHC/SPI ratio was 1:16, the SPI molecules were relatively excessive to the CHC molecules, leading

183 to a decrease in the optimal turbidity. This finding is similar to that of Niu et al. [21],
184 who found that the turbidity curve of ovalbumin/acacia composite solutions shifted to
185 a higher pH value with the increase of ovalbumin/acacia ratio.

186 According to the changing trend of turbidity, the system can be divided into four
187 phase zones: A (co-soluble zone), B (soluble zone), C (insoluble zone), and D (co-
188 insoluble zone). In zone A, the turbidity of the composite solution was almost
189 unchanged, indicating that there was no interaction between SPI and CHC [22]. In zone
190 B, turbidity of the solution increased with the increase of pH, indicating that negatively
191 charged carboxyl group on SPI protein combined with the positively charged amino
192 group of chitosan, forming the soluble SPI-CHC complex in the pH range of pHc-pHφ1.
193 In zone C, the turbidity increased rapidly when the pH value of the solution was greater
194 than pHφ1, indicating the formation of insoluble complexes. In the case of CHC/SPI
195 ratio 1:8, the maximum turbidity was observed at pH_{opt} (6.1), after which the turbidity
196 decreased. This is because the repulsion between SPI and CHC was weakened and the
197 complex coacervation led to phase separation. The change in turbidity of the composite
198 solution in zone D was small, but the overall turbidity value was greater than that in
199 zone A. This is because the pH value of the composite system is close to the pKa of
200 CHC, and its protonation degree decreases, leading to an increase of the turbidity [23].

201 The interactions between SPI and CHC were further analyzed by the investigation
202 of zeta-potential change of SPI-CHC complexes at different pH values and different
203 ratios of CHI/SPI. As presented in Fig.1b, with the increase of pH value from 2 to 9,
204 the zeta-potential of SPI was decreased from +25 mV to -23.56 mV. At pH 4.5, the zeta-

potential was zero, indicating the isoelectric point of SPI. The zeta-potential of CHC solution did not change significantly from pH 2 to 4, but decreased continuously from pH 4 to 9. When the pH value of CHC-SPI composite solution (ratio 1:8) increased from 2 to 9, the zeta-potential was decreased from +30.45 mV to -11.61 mV, and the zeta-potential was zero at 6.2, which corresponded to the pH_{opt} point (6.1, see Fig. 1a). With the increase of pH value, SPI was negatively charged, while CHC was always positively charged at pH 2-9, thus the complex coacervation of SPI and CHC was driven by the electrostatic interaction between them. The soluble complexes were formed because the complexes were still positively charged and electrostatic repulsion prevented further aggregation between the particles. With the increase of pH value, the negative charge of the SPI was increased, which reduced the charge of the complexes, and enhanced electrostatic attraction, leading to the aggregation and precipitation of the complexes. When $pH=pH_{opt}$, the complex coacervation was the strongest.

The particle concentration of CHC and SPI also affects their interaction between them. As an example, in the case of CHC/SPI ratio 1:8, the change in turbidity of composite solutions at total concentration of 0.05%~3% was investigated. As presented in Fig. 1c, the optimal turbidity increased with the increase of particle concentration. The optimum turbidity value increases with the increase of particle concentration. When the particle concentration increased from 0.05% to 3%, the optimum turbidity value was increased from 0.666 to 3.793. When the particle concentration increased from 0.05% to 2%, the optimal turbidity value was increased faster, and when the particle concentration increased from 2% to 3%, the increasing rate of turbidity was

become slower. This is because the increase of concentration lead to the release of more anti-equilibrium ions in the system. These ions shielded the charged sites on the surface of protein and polysaccharide molecules, which hindered the complex coacervation between these molecules.

The particle size and PDI also reflect the stability of complexes formed by SPI-CHC composite solutions. PDI is an index characterizing the homogeneity of particle size distribution. As shown in the Fig. 2, in the case of CHC/SPI ratio1:8, at pH value of <5, the particle size of the composite solution was relatively small, and decreased with the reduction of pH value. At a lower pH value, although polysaccharides and proteins bind together, they have electrostatic repulsion due to the same charge, and the repulsion increases with the decrease of pH value until they dissociate [24]. Low PDI value generally indicates a good particle dispersion. When the pH value was 5-8, the electrostatic attraction between SPI and CHC resulted in the decrease of particle charge while increase of particle size, which led to phase separation and instability of the system. With the further increase of pH value, particle size decreased sharply but PDI was large. This is because the decrease of CHC protonation degree led to the particle aggregation or precipitation [25].

3.2 Efficiency of encapsulation

Encapsulation and loading rate are important indices for quality control of nanoparticles and reflect the percentage of drug entrapped by the carrier, thus determining whether the vehicle is suitable for application as a carrier [26]. Therefore, the encapsulation efficiency (EE) and loading rate (LR) of different concentrations of

249 rutin encapsulated in SCR microcapsules were studied (Table 1). When the
250 concentration of rutin reached 200 mg/L, the EE and LR of SCR microcapsules reached
251 the maximum, being 90.34 ± 2.70% and 0.51 ± 0.03%, respectively. The reduced EE
252 and LR in the high rutin concentration (>200 mg/L) could be attributed to the limited
253 space and particle size within the nanocomposites, excessive rutin did not increase the
254 loading rate but rather destabilized the entire system. Li et al. [27] embedded curcumin
255 in SPI by pH driving method, and the embedding rate was 80.84%. In a recent report,
256 in which SPI and sodium alginate nanoparticles were used for targeted delivery of
257 curcumin, the EE and LR were found as 99.86% and 0.60% [28].

258 **3.3 Infrared spectrum analysis**

259 FT-IR spectra were used to analyze the interaction between rutin and SPI and CHC
260 in the microcapsules. The infrared spectrum of CHC (Fig. 3a) showed the typical
261 characteristic absorption peaks at 3403 cm^{-1} and 2918 cm^{-1}, which corresponded to the
262 stretching vibration of O-H and C-H in turn. The vibration caused by $-NH_3^+$ at 1516
263 cm^{-1} was the key proof of the hydrochloride of chitosan. The absorption peaks at 1379
264 cm^{-1} and 1085 cm^{-1} are caused by the symmetric deformation vibration of CH_3 and the
265 stretching vibration of C-OH in the amide III band [29]. In the infrared spectrum of SPI
266 (Fig. 3b), the absorption peaks appearing at 1655.76 cm^{-1}, 1536.11 cm^{-1} and 1397.24
267 cm^{-1} were caused by C=O stretching vibration of free carboxyl groups, N-H
268 deformation vibration (amide II band) and C-N stretching vibration (amide III band).
269 In the infrared spectrum of SC (Fig. 3c), the amide I, II and III bands shifted to 1656.07
270 cm^{-1}, 1530.97 cm^{-1} and 1387.63 cm^{-1}, respectively, when compared to SPI; compared

to CHC, the disappearance of the characteristic absorption peak of -NH_3^+ proved the existence of electrostatic interaction between SPI and CHC, which led to the aggregation of SPI and CHC [15]. In addition, the band between 3100-3500 cm^{-1} reflects the formation and change of hydrogen bonding, thus the increase in intensity of absorption peak at 3296.94 cm^{-1} in the IR spectra of SC indicated that the interaction between CHC and SPI was also related to hydrogen bonding [30].

The IR spectrum of rutin (Fig. 3d) had a weak absorption at 3422.56 cm^{-1} belonging to the stretching vibration of O-H, a C=O absorption peak at 1654.97 cm^{-1}, an aromatic C=C absorption at 1503.75 cm^{-1}, a phenolic group absorption at 1361.52 and 1294.07 cm^{-1}, 1202.87 cm^{-1} and 1062.71 cm^{-1} were C-O-C absorption peaks [15]. There were two C-O-C absorption peaks change in the IR spectrogram of SCR (Fig. 3e), the stretching vibration of O-H moved to 3420.74 cm^{-1}, the intensity of the absorption peaks of phenolic groups decreased, indicating the formation of hydrogen bonds in SCR and the chemical stability of rutin inside the cavity [30]. Compared with SC, the position of the O-H band in the IR spectrum of SCR moved from 3296.94 cm^{-1} to 3420.74 cm^{-1}, which was attributed to the hydrogen bonding between the rutin and SC complex. It was noted that in the IR spectrum of SCR, most of the characteristic absorption peaks of rutin disappeared, which could be because the stretching vibration of rutin molecule was limited after complexing with SC, which indicated that rutin was encapsulated in SC complex [31]. For instance, the peak at 1656 cm^{-1} in the IR spectra of SC (Fig. 3c) and the peaks at 1654 and 1592 cm^{-1} in the IR spectra of lutin (Fig. 3d) disappeared in the IR spectra of SCR (Fig. 3e), while a new peak appeared at 1649 cm^{-}

293 [1]. This result is similar to that of a previous report [15], where the FTIR spectra of the
294 physical mixture of quinoa starch and rutin was reported to have peaks at 1652 and
295 1594 cm^{-1}, but the rutin loaded starch NPs only had an absorption peak at 1654 cm^{-1}.
296 In addition, the peaks at 1503 cm^{-1} in the IR spectra of lutin and 1530 cm^{-1} in the IR
297 spectra of SC disappeared in the IR spectra of SCR, and a new peak appeared at 1517
298 cm^{-1}, which could be attributed to interactions of rutin and SC complex through the
299 phenolic OH groups in the process of encapsulation.
300
301 **3.4 Thermal analysis using differential scanning calorimeter**
302 Differential scanning calormetry (DSC) has great advantages in measuring the
303 thermodynamic properties of macromolecular polymers. The DSC patterns of CHC,
304 SPI and SC complex are presented in Fig. 4a. The influence of the complexation of
305 polysaccharides and proteins on the thermal stability of proteins can be reflected by the
306 change of the absorption temperature of the peak heat flow. This is because the peak
307 heat flow can reflect the strength of the force to maintain the three-dimensional
308 structure of proteins. The higher the peak temperature value, the higher the stability of
309 proteins [32]. SPI was relatively easy to be affected by heating, its thermal denaturation
310 temperature was found to be 100 ℃, while that of CHC was 116 ℃. The absorption
311 peak of SC was found to appear at 118 ℃, indicating that the addition of CHC increased
312 the thermal stability of SPI. This is probably attributed to the structural rearrangement
313 of SPI and CHC after forming a complex, and electrostatic attraction and hydrogen
314 bonding between SPI and CHC, which facilitate the formation of a more stable network

315 structure. This is consistent with the previously reported result that the complex
316 coacervation with polysaccharides enhanced the thermal stability of the protein [33].
317 As presented in Fig. 4b, the maximum absorption peak of rutin, SR, SCR appeared
318 at 186 ºC, 116 ºC, 123 ºC, respectively. The change of peak position (thermal
319 denaturation temperature) indicated that rutin was successfully loaded on SPI and SC.
320 Compared with SR, the increase of thermal denaturation temperature of SCR indicated
321 that the microcapsules prepared by protein/polysaccharide composite had better
322 thermal stability than those prepared by using protein alone. This could be caused by
323 the close interaction between SC complex and rutin, which improved the thermal
324 stability. This finding agrees with a previous study [34].

325 **3.5 Microstructural analysis**

326 The surface morphology of CHC, SPI, SC and SCR was observed by SEM (Fig.
327 5). CHC was found to have a flat and blocky form, with a very rough surface, indicating
328 the existence of high-level structural interaction, thus possessing a good stability [25].
329 SPI was uneven and spherical, with an inwardly concave and aggregated surface. The
330 SC showed a block shape with a rough surface; in the magnified image, a porous
331 network structure spaced with different size of vacuoles were clearly observed on the
332 blocky surface. Compared with the porous network structure of the SC complex, the
333 surface of SCR was multidimensional. Rutin could be encapsulated in the hydrophobic
334 cavities provided by SC to form the microcapsules. This finding is consistent with that
335 of Huang et al. [35].

336 **3.6 Storage stability of SCR microcapsules**

Fig. 6a shows the changes of particle size and PDI of the samples during the 12 d-storage at 4°C. The particle size of SCR was found to increase slightly from 0 to 3 d and then remained almost unchanged in the following 9 d, with an increase of only 72 nm over the whole storage period. The particle size of SC was fluctuated during the storage period, with an overall increase of 115 nm, but no significant flocculation occurred during the whole storage period. These results indicated that both SCR and SR had good stability, and the stability of SCR was better than that of SR microcapsules. The slight fluctuation in the size of the microcapsules could be caused by the collisions between a small amount of nanoparticles. The PDI of the both samples remained below 0.7 during the period of a 12 d-storage, indicating that the size distribution of the SC and SCR microcapsule solutions was relatively uniform.

As presented in Fig. 6b, the turbidity of both the re-dissolved solutions of SC and SCR microcapsule powder changed very little during the 12d-storage period at 4°C, which was consistent with the phenomena that no obvious flocculation was observed. The zeta-potential of both solutions did not fluctuate significantly during storage, changing from 21.07 ± 0.40 mV to 20.9 ± 1.13 mV for SC and from 26.57 ± 1.37 mV to 22.73 ± 1.28 mV for SCR, respectively. The uniform dispersion of the re-dissolved solutions of SC and SCR microcapsules could be maintained by the electrostatic mutual repulsion between the particles due to positively charged SC and SCR particles [36]. The above results indicated that both SC and SCR microcapsules exhibited a good storage stability, and the storage stability of SCR microcapsules was better than that of SR microcapsules.

3.7 Release behavior of rutin from microcapsules

The release profile of rutin from rutin-loaded microcapsules in the gastrointestinal tract is critical for their application. The physical structure of the rutin-loaded microcapsules can affect their physicochemical properties such as the dissolution rate, apparent solubility and released profile. In this study, the rutin release behavior of SCR under simulated gastrointestinal conditions was investigated in comparison with that of SR. As illustrated in Fig.7, the amount of rutin released from both SR and SCR microcapsules was relatively low during the first hour of digestion in the simulated gastric fluid. This is because the interaction between rutin and protein can protect protein from pepsin digestion to a certain extent, resulting in a delay in digestion [28]. In the second hour, rutin was released rapidly from SR microcapsules, while the release of rutin from SCR microcapsules still remained at low speed. The cumulative release rate of rutin from SR microcapsules was 58.29%, being significantly higher than that of SCR (18.21%) during the 2h digestion in the simulated gastric juice. This is because the peptide bond between hydrophobic amino acid in the protein shell of SR microcapsules was hydrolyzed by pepsin, leading to a damage of protein structure, and consequently speeding up the release of rutin. In contrast, owing to the electrostatic attraction between protein and polysaccharide, the structure of SPI in SCR was protected from the enzymatic hydrolysis of peptide bonds formed by hydrophobic amino acids [14].

In the simulated intestinal fluid, rutin in SR and SCR were rapidly released, with release rates of 45.24% and 76.53% respectively, indicating that SR and SCR both

effectively released rutin in the intestine, allowing the absorption of rutin by the body. After 4h digestion in the simulated intestinal fluid, the rutin release rate of SR and SCR reached more than 90%, indicating that SCR had a good targeted release effect in the intestine, thus improving the bioavailability of rutin.

3.8 Antioxidant activity of SCR microencapsulated digestion products

The protective effect of microcapsules on the biological activities of rutin during digestion was investigated by examining the antioxidant activity of gastric and intestinal simulated digests of free rutin, SCR and SR (Fig. 8a and 8b). It was found that under both gastric and intestinal simulated conditions, the antioxidant activities of the digests from SCR and SR were significantly ($p < 0.05$) higher than those of uncapsulated rutin. This finding agrees with that of a previous report [15]. The superior antioxidant activity of the digests from SCR and SR to that of free rutin digest could be because more rutin in the digest of free rutin was conversed to quercetin during the digestion [15]. Rutin was reported to possess better DPPH• and $ABTS^{\bullet+}$ scavenging abilities than quercetin [37,38]. Thus, the result in this study indicates the good protection of encapsulation on the bioactivity of rutin. Both DPPH• and $ABTS^{\bullet+}$ scavenging abilities of SR digest in gastric juice were higher than those of SCR digest, while the opposite results were observed for their intestinal digests, which was in agreement with the cumulative release of rutin from SCR and SR in gastric and intestinal simulated juices.

4. Conclusion

Rutin-loaded microcapsules were prepared by complex coacervation using SPI and CHC as encapsulating materials. FT-IR, DSC and SEM analyses demonstrated the successful encapsulation of rutin in the SC complex to form SCR microcapsules, which had small particle size, negative zeta potential and high encapsulation rate. The rutin embedded in SCR microcapsules were able to prevent the digestion by gastric pepsin in stomach but allow rutin to be released from SCR microcapsules in the intestine and to achieve a targeted release effect, thereby improving the bioavailability of rutin. Therefore, the SCR microcapsules developed in this study provide a new application of rutin in medicine and other fields, this paved a foundation for the hydrophobic compounds, like rutin, with high bioactive effect but with lower bioavailability and sensitive to the gastric condition. Further studies are required in the due course, such as the activity *in vivo* and safety evaluation.

CRediT author statement

Shuai Dong: Investigation, Writing-Original draft preparation, data curation.

Shu-Min Hu: Methodology, Investigation, resources.

Si-Jia Yu: Investigation, formal analysis.

Shaobo Zhou: Formal analysis, Writing-Review & Editing.

Tao Zhou: Conceptualization, Supervision, Funding acquisition, Writing-Review & Editing.

Conflicts of Interest

The authors declare no competing interest.

Acknowledgments

This work was supported by “Pioneer” and “Leading Goose” R&D Program of

Zhejiang of China (2022C02012).

References

[1] G. S, Ravi, R. N. Charyulu, A. Dubey, P. Prabhu, S. Hebbar, A. C. Mathias, Nano-lipid Complex of Rutin: Development, Characterisation and In Vivo Investigation of Hepatoprotective, Antioxidant Activity and Bioavailability Study in Rats, AAPS PharmSciTech 19(8) (2018) 3631-3649, https://doi.org/10.1208/s12249-018-1195-9.

[2] R. Mauludin, R.H. Muller, C.M. Keck, Kinetic solubility and dissolution velocity of rutin nanocrystals, Eur J Pharm Sci 36(4-5) (2009) 502-10, https://doi.org /10.1016/j.ejps.2008.12.002

[3] F. Zhu, Encapsulation and delivery of food ingredients using starch based systems, Food Chem 229 (2017) 542-552, https://doi.org/10.1016/j.foodchem.2017.02.101.

[4] N. Devi, M. Sarmah, B. Khatun, T.K. Maji, Encapsulation of active ingredients in polysaccharide-protein complex coacervates, Adv Colloid Interface Sci 239 (2017) 136-145, https://doi. org/10.1016/j.cis.2016.05.009.

[5] P.X. Qin, T.R. Wang, Y.C. Luo, A review on plant-based proteins from soybean: Health benefits and soy product development. J Agri Food Res 7 (2022) 100265, https://doi.org/10.1016/j.jafr.2021.100265

[6] F. P. Chen, B. S. Li, C. H. Tang, Nanocomplexation of soy protein isolate with curcumin: Influence of ultrasonic treatment, Food Res Int 75 (2015) 157-165, https://doi.org/10.1016/j.foodres.2015.06.009.

[7] C.-H. Tang, Nanostructured soy proteins: Fabrication and applications as delivery systems for bioactives (a review), Food Hydrocoll 91 (2019) 92-116, https://doi.org/10.1016/j.foodhyd.2019.01.012.

[8] L. Zhang, F. Zhang, Y. Fang, S. Wang, Alginate-shelled SPI nanoparticle for encapsulation of resveratrol with enhanced colloidal and chemical stability, Food Hydrocoll 90 (2019) 313-320. https://doi.org/10.1016/j.foodhyd.2018.12.042.

[9] D. Wu, L. Tang, Z. Zeng, J. Zhang, X. Hu, Q. Pan, F. Geng, H. Li, Delivery of hyperoside by using a soybean protein isolated-soy soluble polysaccharide nanocomplex: Fabrication, characterization, and in vitro release properties, Food Chem 386 (2022) 132837, https://doi.org/10.1016/j.foodchem.2022.132837.

[10] Y. Yuan, Z. L. Wan, S.W. Yin, X.Q. Yang, J.R. Qi, G.Q. Liu, Characterization of complexes of soy protein and chitosan heated at low pH, LWT-Food Sci Technol 50 (2013) 657–664. https://doi.org/10.1016/j.lwt.2012.07.034.

[11] S.N. Gao, M.Y. Yang, Z.S. Luo, Z.J. Ban, Y. Pan, M.Y. Tu, Q. Ma, X.Y. Lin, Y.Q. Xu, L. Li , Soy protein/chitosan-based microsphere as Stable Biocompatible Vehicles of Oleanolic Acid: An Emerging Alternative Enabling the Quality Maintenance of Minimally Processed Produce, Food Hydrocoll 124 (2022) 107325, https://doi.org/10.1016/j.foodhyd.2021.107325

[12] J.X. Xiao, G.Q. Huang, S.Q. Wang, Y.T. Sun, Microencapsulation of Capsanthin by Soybean Protein Isolate-Chitosan Coacervation and Microcapsule Stability Evaluation, J Appl Polym Sci 131 (2014) 39671, https://doi.org/10.1002/app.39671.

[13] S. Liu, Q. Yang, J. Zhang, M. Yang, Y. Wang, T. Sun, C. Ma, A.M. Abd El-Aty, Enhanced stability of stilbene-glycoside-loaded nanoparticles coated with carboxymethyl chitosan and chitosan hydrochloride, Food Chem 372 (2022), https://doi.org/10.1016/j.foodchem.2021.131343.

[14] Y.-Y. Xu, Y.-F. Huo, L. Xu, Y.-Z. Zhu, Y.-T. Wu, X.-Y. Wei, T. Zhou, Resveratrol-loaded

ovalbumin/Porphyra haitanensis polysaccharide composite nanoparticles: Fabrication, characterization and antitumor activity, J Drug Deliv Sci Technol 66 (2021) 102811, https://doi.org/10.1016/j.jddst.2021.102811.

[15] M. K. Remanan, F. Zhu, Encapsulation of rutin using quinoa and maize starch nanoparticles, Food Chem 353 (2021), https://doi.org/10.1016/j.foodchem.2020.128534.

[16] Y.Z. Zhu, K. Chen, Y.L. Chen, C.J. Zhang, Y.Y. Xie, R. C. Hider, T. Zhou, Design, synthesis of novel stilbene-hydroxypyridinone hybrids as tyrosinase inhibitors and their application in the anti-browning of freshly-cut apples, Food Chem 385 (2022) 132730, https://doi.org/10.1016/j.foodchem.2022.132730.

[17] X. Zhang, Y.T. Wu, X.Y. Wei, Y.Y. Xie, T. Zhou, Preparation, antioxidant and tyrosinase inhibitory activities of chitosan oligosaccharide-hydroxypyridinone conjugates, Food Chem 420 (2023) 136093, https://doi.org/10.1016/j.foodchem.2023.136093.

[18] C. Xiang, J. Gao, H. Ye, G. Ren, X. Ma, H. Xie, S. Fang, Q. Lei, W. Fang, Development of ovalbumin-pectin nanocomplexes for vitamin D3 encapsulation: Enhanced storage stability and sustained release in simulated gastrointestinal digestion, Food Hydrocoll 106 (2020), https://doi.org/10.1016/j.foodhyd.2020.105926.

[19] M.-M. Wang, F. Wang, G. Li, M.-T. Tang, C. Wang, Q.-Q. Zhou, T. Zhou, Q. Gu, Antioxidant and hypolipidemic activities of pectin isolated from citrus canning processing water, Lwt 159 (2022).

[20] M. Klein, A. Aserin, P.B. Ishai, N. Garti, Interactions between whey protein isolate and gum Arabic, Colloid Surface B 79(2) (2010) 377-383, https://doi.org/10.1016/j.lwt.2022.113203.

[21] F. Niu, J. Zhou, D. Niu, C. Wang, Y. Liu, Y. Su, Y. Yang, Synergistic effects of ovalbumin/gum arabic complexes on the stability of emulsions exposed to environmental stress, Food Hydrocoll

492 47 (2015) 14-20, https://doi.org/10.1016/j.colsurfb.2013.08.012.
493 [22] S.N. Warnakulasuriya, M.T. Nickerson, Review on plant protein-polysaccharide complex
494 coacervation, and the functionality and applicability of formed complexes, J Sci Food Agric 98(15)
495 (2018) 5559-5571, https://doi.org/10.1002/jsfa.9228.
496 [23] M.G. Semenova, Thermodynamic analysis of the impact of molecular interactions on the
497 functionality of food biopolymers in solution and in colloidal systems, Food Hydrocoll 21(1)
498 (2007) 23-45, https://doi.org/10.1016/j.foodhyd.2006.02.009.
499 [24] C.-H. Tang, F. Liu, Cold, gel-like soy protein emulsions by microfluidization: Emulsion
500 characteristics, rheological and microstructural properties, and gelling mechanism, Food
501 Hydrocoll 30(1) (2013) 61-72, https://doi.org/10.1016/j.foodhyd.2012.05.008.
502 [25] N.C. Minh, V.H. Nguyen, S. Schwarz, W.F. Stevens, T.S. Trung, Preparation of water soluble
503 hydrochloric chitosan from low molecular weight chitosan in the solid state, Int J Biol Macromol
504 121 (2019) 718-726. https://doi.org /10.1016/j.ijbiomac.2018.10.130.
505 [26] H. Li, D. Wang, C. Liu, J. Zhu, M. Fan, X. Sun, T. Wang, Y. Xu, Y. Cao, Fabrication of stable
506 zein nanoparticles coated with soluble soybean polysaccharide for encapsulation of quercetin,
507 Food Hydrocoll 87 (2019) 342-351, https://doi.org/10.1016/j.foodhyd.2018.08.002.
508 [27] H. Li, X. Zhang, C. Zhao, H. Zhang, Y. Chi, L. Wang, H. Zhang, S. Bai, X. Zhang, Entrapment
509 of curcumin in soy protein isolate using the pH-driven method: Nanoencapsulation and formation
510 mechanism, LWT-Food Sci Technol 153 (2022) 112480,
511 https://doi.org/10.1016/j.lwt.2021.112480.
512 [28] S. Shahbazizadeh, S. Naji-Tabasi, M. Shahidi-Noghabi, Entrapment of curcumin in isolated
513 soy protein-alginate nanogels: antioxidant stability and in vitro gastrointestinal digestion, J Food

514 Meas Charact 16(6) (2022) 4754-4770, https://doi.org/10.1007/s11694-022-01562-4.
515 [29] C. Sun, L. Dai, Y. Gao, Formation and characterization of the binary complex between zein
516 and propylene glycol alginate at neutral pH, Food Hydrocoll 64 (2017) 36-47.
517 [30] M.H. Asfour, A.M. Mohsen, Formulation and evaluation of pH-sensitive rutin nanospheres
518 against colon carcinoma using HCT-116 cell line, J Adv Res 9 (2018) 17-26,
519 https://doi.org/10.1016/j.foodhyd.2016.10.031.
520 [31] Q. Guo, I. Bayram, W. Zhang, J. Su, X. Shu, F. Yuan, L. Mao, Y. Gao, Fabrication and
521 characterization of curcumin-loaded pea protein isolate-surfactant complexes at neutral pH, Food
522 Hydrocoll 111 (2021) 106214, https://doi.org/10.1016/j.foodhyd.2020.106214.
523 [32] C.-H. Tang, X.-R. Li, Microencapsulation properties of soy protein isolate: Influence of
524 preheating and/or blending with lactose, J Food Eng 117(3) (2013) 281-290.
525 https://doi.org/10.1016/j.jfoodeng.2013.03.018.
526 [33] Y. Zhong, L. Yang, D.J. McClements, X. Wang, J. Ye, C. Liu, Spray drying and rehydration of
527 macadamia oil-in-water emulsions: Impact of macadamia protein isolate to chitosan
528 hydrochloride ratio, Food Chem 342 (2021) 128380,
529 https://doi.org/10.1016/j.foodchem.2020.128380.
530 [34] Z. Zhang, G. Hao, C. Liu, J. Fu, D. Hu, J. Rong, X. Yang, Recent progress in the preparation,
531 chemical interactions and applications of biocompatible polysaccharide-protein nanogel carriers,
532 Food Res Int 147 (2021) 110564, https://doi.org/10.1016/j.foodres.2021.110564.
533 [35] G.Q. Huang, Y.T. Sun, J.X. Xiao, J. Yang, Complex coacervation of soybean protein isolate
534 and chitosan, Food Chem 135(2) (2012) 534-9, https://doi.org/10.1016/j.foodchem.2012.04.140.
535 [36] C. Qiu, M. Zhao, D.J. McClements, Improving the stability of wheat protein-stabilized

emulsions: Effect of pectin and xanthan gum addition, Food Hydrocoll 43 (2015) 377-387, https://doi.org/10.1016/j.foodhyd.2014.06.013.

[37] Y.M. Zhou, H.Y. Duan, J.S. Chen, S.J. Ma, M.L. Wang, X.L. Zhou, The mechanism of in vitro non-enzymatic glycosylation inhibition by Tartary buckwheat's rutin and quercetin, Food Chem 406 (2023) 134956, https://doi.org/10.1016/j.foodchem.2022.134956.

[38] A. Alper Öztürk, E. Başaran, B. Şenel, M. Demirel, Ş. Sarıca, Synthesis, characterization, antioxidant activity of Quercetin, Rutin and Quercetin-Rutin incorporated β-cyclodextrin inclusion complexes and determination of their activity in NIH-3T3, MDA-MB-231 and A549 cell lines, J Mol Struct 1282 (2023) 135169, https://doi.org/10.1016/j.molstruc.2023.135169

Tables

Table 1. Encapsulation efficacy (EE) and loading rate (LR) of SCR microcapsules at different concentration of rutin

Rutin (mg/L)	EE (%)	LR (%)
20	86.89±4.39[a]	0.32±0.04[a]
40	89.00±3.47[b]	0.35±0.06[a]
200	90.34±2.70[b]	0.51±0.03[b]
400	61.18±2.36[b]	0.49±0.06[b]

Different alphabets denote significant difference ($p < 0.05$) between the different groups (mean ± standard deviation, n = 3).

Figure captions

Figure 1. Effects of pH and SPI/CHC ratio on the turbidity of SPI-CHC complex solution (a); zeta potential of SPI, CHC and SPI-CHC complex (b); effect of CHC/SPI concentration on turbidity of composite system (c).

Figure 2. Effect of pH on size of SPI-CHC complex solution (a)， and PDI of SPI, CHC and SPI-CHC complex (b).

Figure 3. FT-IR spectra of CHC (a), SPI (b), SC (c), rutin (RUT) (d), and SCR (e).

Figure 4. The DSC patterns of SPI, CHC, SC (a); and RUT, SR, SCR (b).

Figure 5. SEM of CHC (a), SPI (b), SC (c) and SCR (d).

Figure 6. Storage stability of SC and SCR. (a) Particle size and PDI; (b) zeta-potential and turbidity. Different letters indicate the significant difference within the same group ($p < 0.05$).

Figure 7. Simulated release of SR and SCR *in vitro*.

Figure 8. Antioxidant activity of digestion products of microcapsules. (a) DPPH· scavenging ability; (b) $ABTS^{\bullet+}$ scavenging ability. Bars with different letters above within the same group differ significantly ($p < 0.05$).

572 **Fig.1**

573 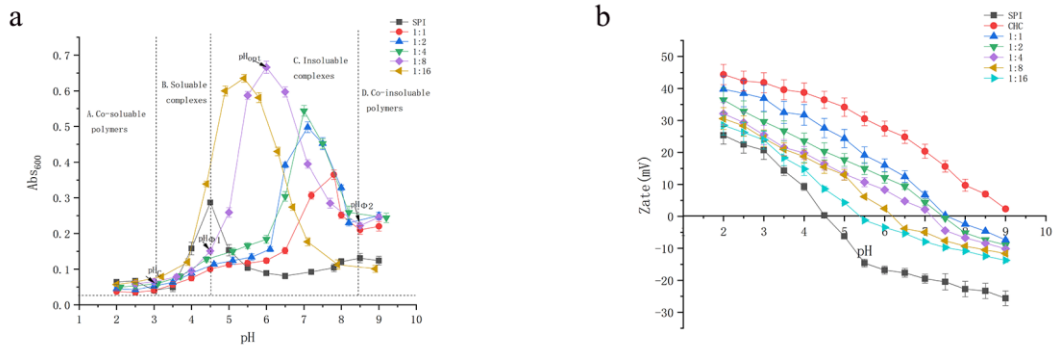

574 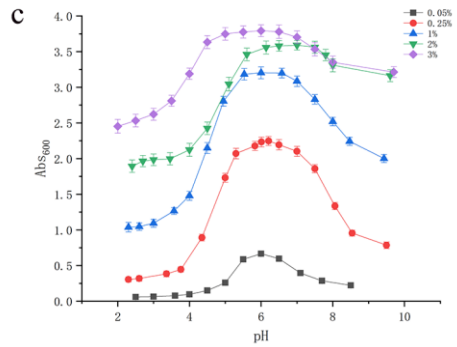

575 **Fig.1**. Effects of pH and SPI/CHC ratio on the turbidity of SPI-CHC complex solution

576 (a); and zeta potential of SPI, CHC and SPI-CHC complex (b); effect of CHC/SPI

577 concentration on turbidity of composite system (c).

578

579 **Fig.2**

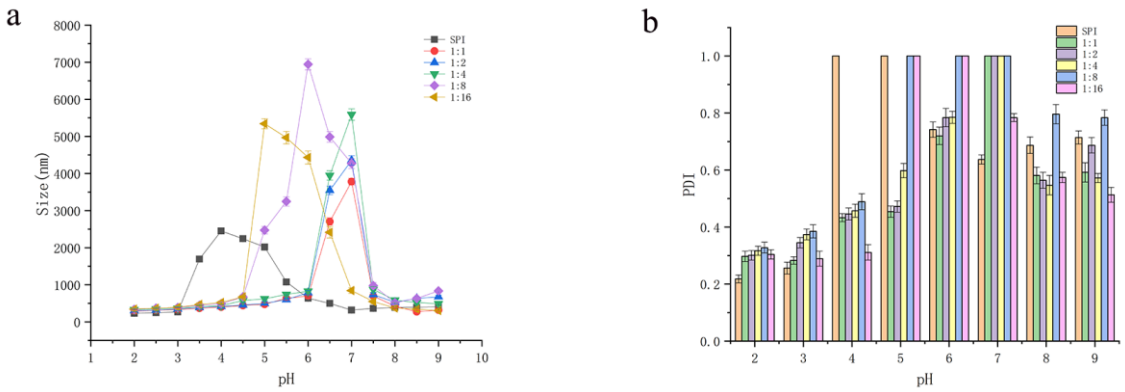

580
581

582 **Fig. 2.** Effect of pH on size of SPI-CHC complex solution (a), and PDI of SPI, CHC

583 and SPI-CHC complex (b).

584
585

Fig.3

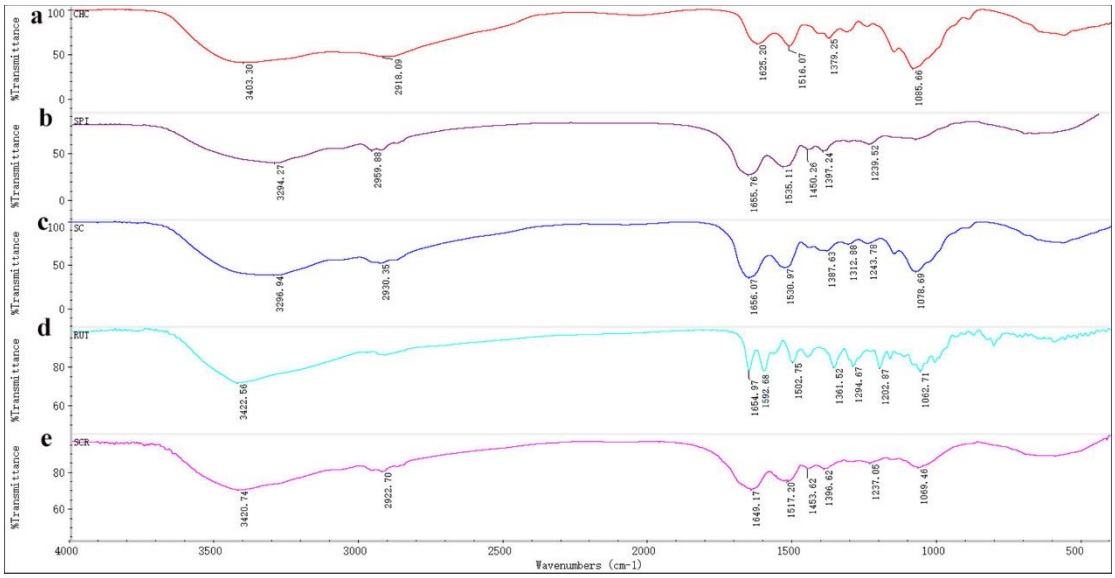

Fig.3. FT-IR spectra of CHC (a), SPI (b), SC (SPI-CHC) (c), rutin (RUT) (d), and SCR (SPI-CHC-RUT) (e).

591 Fig.4

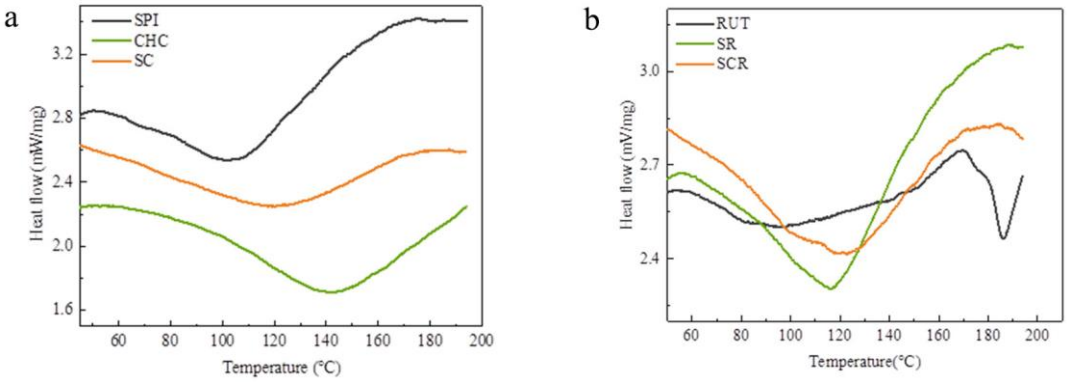

592

593 **Fig. 4**. The DSC of SPI, CHC, SC (a); and rutin (RUT), SR (SPI-RUT), SCR (SPI-

594 CHC-RUT) (b).

595

596

597 **Fig.5**

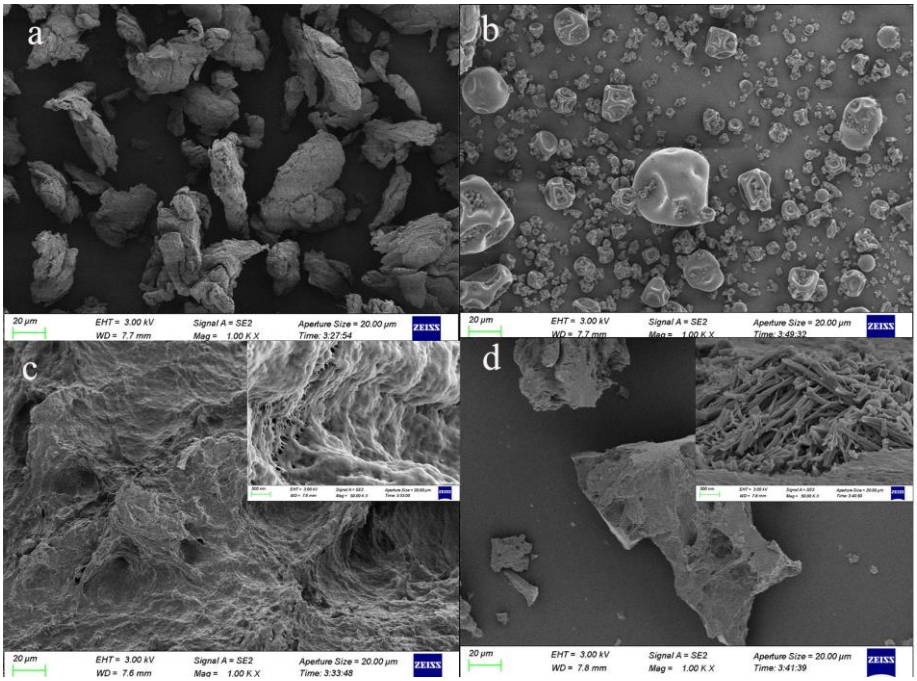

598

599 **Fig.5**. SEM of CHC (a), SPI (b), SC (c) and SCR (d).

600

Fig.6

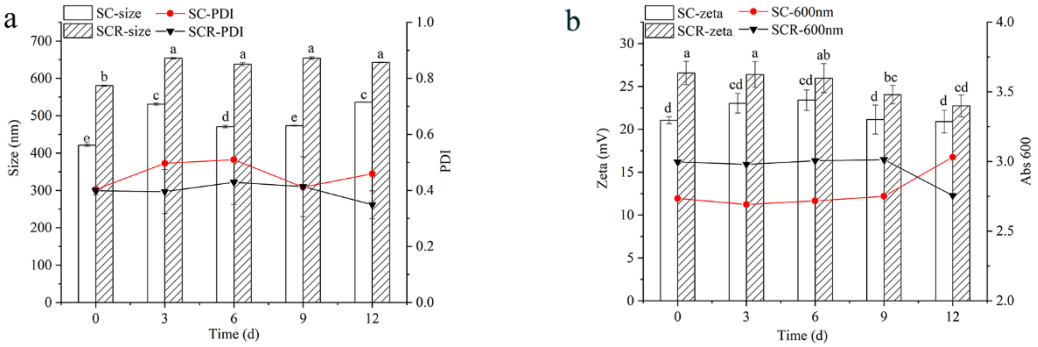

Fig. 6. Storage stability of SC and SCR. (a) Particle size and PDI; (b) zeta potential and turbidity. Different letters indicate the significant difference within the same group ($p < 0.05$).

607 **Fig.7**

608

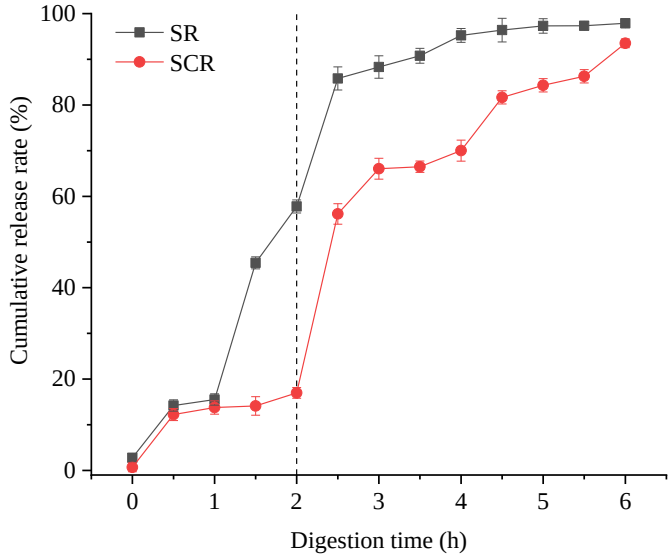

609

610 **Fig.7**. Simulated release of SR and SCR *in vitro*

611

612

Fig.8

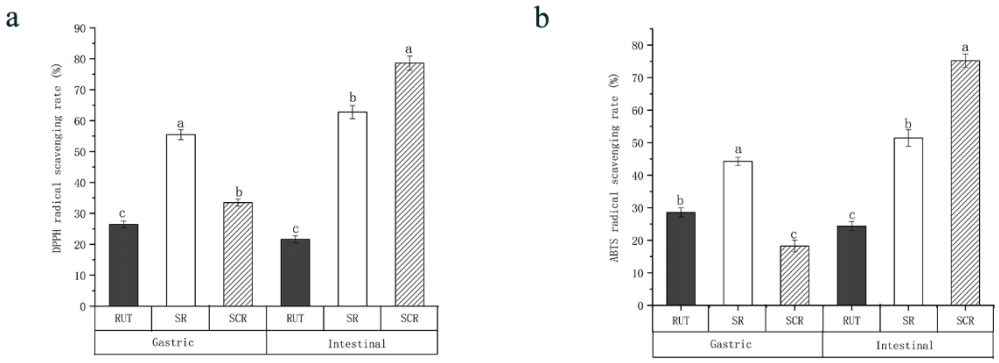

Fig.8. Antioxidant activity of digestion products of microcapsules. (a) DPPH· scavenging ability; (b) $ABTS^{\bullet+}$ scavenging ability. Bars with different letters above within the same group differ significantly ($p < 0.05$).